Geomagnetically Induced Currents in the UK: Geomagnetic Variations and Surface Electric Fields

D. Beamish[1], T. D. G. Clark[2,*], E. Clarke[2] and A. W. P. Thomson[2]

[1] British Geological Survey, Keyworth, Nottingham, NG12 5GG,UK.
[2] British Geological Survey, West Mains Road, Edinburgh, EH9 3LA, UK.
[*] Corresponding author (fax: +44 131 668 4368; e-mail: t.clark@bgs.ac.uk)

Abstract

The geomagnetically induced current (GIC) risk to the power transmission grid in the United Kingdom is discussed with reference to an example of a geomagnetic storm during which GICs were suspected of causing abnormal transformer behaviour. A simple measure of the power of the magnetic field variation, the hourly standard deviation (HSD) in the north or east horizontal component, is used to determine the general risk to the UK power grid from rapid magnetic variations, according to season and local time. Monitoring and forecasting of HSD may be a useful means of gauging the likely risk to high-cost power engineering equipment. A simplified but representative three-dimensional geological model of the UK landmass and surrounding seas is used to provide an indication of the surface electric field for various amplitudes and orientations of external magnetic field variations. It is found that the resistivity contrast between seawater and the onshore geology, particularly around the Scottish metamorphic terranes, produces enhanced electric fields at coastal sites. These are as much as 4 V/km for a 1 A/m (or 1257 nT) external field with 10 minute period.

1. Introduction

Electric fields are induced in the Earth, and in conductors at or near the surface of the Earth, by variations in the strength and direction of the geomagnetic field. These electric fields drive currents called geomagnetically induced currents (GICs). GICs have been studied since the mid-19th century when their effects on long distance telecommunication cables were first noticed. These currents can adversely affect electrical power transmission grids, saturating transformers by flowing through the earthed neutral line, leading to possible overheating, generation of harmonics and increased reactive load. The effects of GICs on power transmission systems have been extensively studied in recent years following the catastrophic failure of the power transmission grid in Quebec during a severe geomagnetic disturbance on the night of 13/14 March 1989. A description of this event and subsequent work to reduce the GIC risk on the Quebec grid is given by Blais and Metsa (1994). Previous theoretical and experimental modelling work on GICs includes that of Boteler and Pirjola (1998), Viljanen (1997), Pirjola and Viljanen (1998) and Viljanen and Pirjola (1994).

During times of intense magnetic activity the British Isles, lying between geomagnetic latitudes 53°N and 62°N, can experience strong magnetic disturbances under the

expanded auroral oval. The peak of the current sunspot cycle is predicted to be around the year 2000 (Joselyn et al., 1997). Given that in most previous solar cycles the level of geomagnetic activity increases in the three to four years following solar maximum, it is now timely to examine the hazard to power transmission posed by GICs in the UK.

The transmission grid in England and Wales, operated by the National Grid Company (NGC), is connected to the Scottish grid, in which the southern part is operated by ScottishPower and the northern part by Scottish Hydro-Electric.

To understand the potential problem facing power companies in the British Isles, the following major influences on the risk posed by GICs to the transmission grid must be examined:

1. The timing, frequency and severity of geomagnetic storms (ie. climatology);

2. Spatial variations in the resistivity structure of the British Isles and its associated continental shelf and seas;

3. The electrical network characteristics of the transmission grid and its response to the surface electric field to which it is exposed.

This paper examines aspects of the climatology of storms and the resistivity of the British Isles. We provide both a statistical overview of UK geomagnetic disturbances and also examples of modelled surface electric fields that result from idealised ionospheric magnetic fields. A study of the third influence - the grid response to these electric fields - requires long-term, routine monitoring of GICs within the UK power network by the system operators and power companies, complemented with system studies. Although there is little published data on GICs in the UK grid (see, for example, Smith, 1990) this is a vital component of the problem as it allows theoretical models to be tested.

The vector components of the geomagnetic field are measured continuously at the three UK geomagnetic observatories, situated at Lerwick (in Shetland), Eskdalemuir (in the Scottish Borders) and Hartland (in Devon) – see Figure 1. Digital data are available as one-minute mean values from 1983 onwards. There are only about half a dozen events in the past two decades known to us in which GICs have been known to have a measurable effect, of the order of a few amps, in the UK transmission grid. In Section 2 we describe one of these events, in which an attempt was made to measure GICs directly. From this analysis a useful index of geomagnetic activity, the hourly standard deviation in the X (North) and Y (East) components of the geomagnetic field, is then used to characterise the risk, by season and by local time. In Section 3 we outline a resistivity model of the British Isles and surrounding area which is used for estimating the surface electric fields that result from varying magnetic fields. Example computations are given for magnetic fields polarised in the north and east directions at two different frequencies.

2. GICs and Geomagnetic Variations in the UK

2.1 Case study of a magnetic storm correlated with GICs

There is little published data concerning GICs in the British Isles. One example of GICs recorded at NGC transformers on the 20 October 1989 at three locations in England and Wales is discussed by Smith (1990). The current in the transformer neutrals was seen to vary from approximately +5A to -2A at Norwich Main in East Anglia, Pembroke in Wales, and Indian Queens in Cornwall, between 1820UT and 1830UT. The GIC in the eastern location was of opposite phase to that in the western locations. Smith (1990) also gives some anecdotal evidence of GIC effects during the storm of 13-14 March 1989. Increased harmonic content was measured in a transformer at Harker in the north of England during a magnetic storm on 8-9 November 1991 (J. Laver, National Grid Company, personal communication, 1998). A voltage dip in the Scottish grid was linked with a magnetic storm on 13-14 July 1982 (South of Scotland Electricity Board unpublished report).

Here we present a case study of an event identified in the Scottish part of the transmission grid on 17th November 1989. ScottishPower had installed a transformer earth current recorder at the Neilston 400kV substation near Paisley (R. Paton, ScottishPower plc, personal communication, 1992). The data available for 17-18 November 1989 are shown in Figure 2a and consist of an analogue pen-chart recording of three signals and show a period of transformer earth current activity between about 1600UT and 2200UT, with a period of maximum activity in which currents reached 5A just before 1800UT (although there is some doubt about the calibration of the current measurement). The currents varied in positive and negative directions, and there was a further period of enhanced activity around 2100UT. The location of the Neilston substation is shown in Figure 1, in relation to the UK magnetic observatories.

Figure 2b shows the instantaneous rate of change of the X (North) component of the field for the two days of 17-18 November 1989, to be compared with the GIC in Figure 2a. In Figure 2b the three panels show the measurements made at each of the three observatories. It can be seen that the maximum range in the rate of change of the X component occurred at Eskdalemuir (the Y component behaved similarly). It was observed that this storm started with a storm sudden commencement, an initial rapid variation that results from enhanced current systems following the impact of a coronal mass ejection on the Earth's magnetosphere. Recalling that the period of GIC activity observed during this time at Neilston was between 1600-2200UT with a maximum at about 1800UT and a lesser maximum at about 2100UT, we can immediately see some correspondence with the variation of the rate of change of the magnetic field.

2.2 Statistics of magnetic storms in the British Isles 1983-1998

This detailed example and the other events outlined above give a qualitative idea of the magnitude of magnetic disturbances that may give rise to GICs in the British Isles. In order to quantify the occurrence of storms of this type we have examined the hourly standard deviations (HSD) of the X and Y components for the years 1983 to 1998. This choice of parameter is made because the instantaneous electric field does not depend

simply on the instantaneous rate of change of the magnetic field, but more generally on the rate of change integrated over some time interval, as discussed by Cagniard (1953). The maximum rate of change of the magnetic field is therefore not necessarily the best indicator of the size of any induced electric field. For a time series with zero mean, Parseval's theorem equates the variance in the time domain with the integrated spectral power in the frequency domain. Thus the standard deviation (square root of the variance) in the magnetic field, over some interval in the time domain, acts as an indicator of the total magnetic spectral power during that interval. The magnetic spectral power is significant, in turn, because it affects the electric field spectrum through the magnetotelluric relation (Cagniard, 1953). Alternatively, simple geomagnetic indices, the observatory K indices, based on measurements of the range in the horizontal components, exist for various observatories in the British Isles from 1868 onwards. Boteler (1998) has shown that there is a high correlation between range indices and spectral power, and so an approximate relation can be established between K indices and spectral power. However, as one-minute digital data are available from the UK observatories, it is straightforward to compute the standard deviation in the horizontal components directly. A time-scale of one hour is chosen here because this is similar to the duration of magnetic substorms, which are periods of intense magnetic variation at auroral latitudes, and which typically last some tens of minutes to a few hours. (The time scale of the observatory K indices is 3 hours).

The HSD in the X and Y components for the Neilston case study are shown in Figures 3a and 3b. It is clear that the peaks in the HSD index coincide with the intervals of maximum rate of change, and that these also coincide with the times of GIC activity in the Neilston transformer. To examine how often this level of magnetic activity occurs in the years for which digital one-minute data are available (1983 to the present) we have examined how often the HSD exceeds a specified threshold value. It was decided to choose a single threshold for all three observatories to highlight the latitude dependence of geomagnetic activity. The threshold was chosen with reference to all the known GIC 'events'. An appropriate value, which was exceeded at all three UK observatories during each event, is 50 nT.

To study the number of significant events we cannot simply count the number of days on which the threshold was exceeded. This is because many magnetic storms occur over midnight and may result in two days being counted even though only one magnetic storm occurs. Furthermore some short substorm events can exceed the threshold more than once a day, but be separated by some hours of quieter activity. These should therefore be regarded as separate events. Therefore we define a 'GIC-type' storm as a period when HSD (in X or Y) exceeds the threshold of 50 nT, and storms are counted as separate if the HSD drops below the threshold for more than 6 hours between threshold crossings. The threshold and duration criteria are applied separately for the X and Y components at each observatory for the years 1983-1998. The maximum HSD for each day throughout these years is plotted in Figure 4. The dates on which known GIC events were observed, as discussed above, are indicated by dashed vertical lines.

It will be seen from Figure 4 that HSD during a 'GIC-type' storm can reach several hundred nT. For example, the largest storm measured at Eskdalemuir occurred on 9th February 1986, during a time of solar *minimum* activity, when HSD reached 473.5 nT in the *X* component. The storms related to the few known GIC events had a peak HSD which exceeded 50 nT at all three observatories, however the peak HSD was usually substantially higher for the two northern observatories, being typically over 150 nT at Eskdalemuir, and over 200 nT at Lerwick. However the lower threshold of 50 nT may remain significant in terms of degradation, that is, low-level effects integrated over time. It is worth noting that although the maximum HSD is generally greater in the *X* component than the *Y* component, there are still occasions when it can reach values of 200 nT in the *Y* component. During some of the more severe storms the HSD is greater at Eskdalemuir than Lerwick (but note that data from Lerwick were not available for the storm of February 1986).

The number of 'GIC-type' storms per year in the *X* component of the field is shown in Figure 5. This shows the following important points.

1. The 11-year solar cycle is clearly visible in the occurrence of magnetic storms. It is expected that levels of activity similar to 1989-91 will be seen in the years 2000-2003. The double peaks in magnetic activity that have been noticed in many solar cycles are apparent in 1989 and 1991.

2. The number of times the threshold is exceeded in the British Isles is clearly dependent on latitude. As discussed previously this is due to the proximity of the auroral oval at higher latitudes. During years of maximum magnetic activity there are typically ten occasions when the threshold is exceeded at all three observatories, and two or three such events can be expected even during years of low magnetic activity.

3. There is a tendency for more events to occur in the *X* component than the *Y* component, particularly at Lerwick. However the fact that there are a number of events in the *Y* component data (e.g. Figure 4) indicates that when modelling GICs in the grid it is important to consider the effects of GICs induced by magnetic fields polarised in arbitrary directions, rather than simply north-south or perpendicular to some modelled, or 'average', electrojet direction.

The distribution of the duration of these 'GIC-type' storms is shown in Figure 6. Here it can be seen that the majority of storms have a level of activity that exceeds the threshold for less than 3 hours. There are typically only a few storms in a solar cycle which exceed the threshold for more than 24 hours duration. Also of significance is the tendency for severe magnetic activity to occur at a particular local time. Figure 7 shows the hour of day, in Universal Time, at which the peak HSD occurred. There is a clear tendency for activity to occur during night-time hours, a consequence of substorm activity generated by magnetic reconnection in the tail of the magnetosphere.

There is a known tendency for magnetic activity to vary with season. In Figure 8 we show the monthly occurrences of 'GIC-type' magnetic storms summed over the years

1983-1997. More storms occur around March and October, which are times of the year when the average alignment of the geomagnetic field axis throughout the day is most favourable for reconnection with the interplanetary magnetic field.

The results presented here demonstrate the climatology of magnetic storms in the British Isles. Taken with the few examples of GIC events measured in the grid, these results provide information on when the power companies should be concerned about GICs, and which can form the basis of a monitoring service. On the basis of the limited information available, typical HSD thresholds for concern are estimated to be 50 nT at Hartland, 150 nT at Eskdalemuir and 200 nT at Lerwick. However in order to understand the generation of GICs in the grid in detail, which would enable modelling of the grid response to magnetic storms, it is necessary to model the ground resistivity. This is addressed in the next section.

3. Modelled Surface Electric Fields in the UK

3.1 Background to electric field modelling

The electric field (E-field) calculations used in GIC risk assessment typically involve the assumptions: (i) the earth resistivity structure varies only with depth and (ii) the E-field used in engineering calculations is spatially constant. The British Isles have a distinct resistivity structure and are surrounded by shelf-seas. The shelf-seas and deep ocean are known to influence regionally induced electric fields (Beamish, 1985). The present study provides an initial assessment of the limitations of assumptions (i) and (ii) when applied to GIC risk assessment across Britain.

The type of calculation performed when estimating GIC effects in a power grid is described by Viljanen and Pirjola (1994). Induced voltages (V) across power line elements (k to i) are calculated from the surface geoelectric field by a line-integral:

$$V_{ki} = \int_{ki} \mathbf{E \cdot ds} \qquad \qquad …(1)$$

Calculation of the surface E-field in (1) is undertaken using the theory of electromagnetic induction. A geomagnetic variation field is taken as a source and Maxwell's equations are used to calculate the E-field distribution within an appropriate but finite volume of the Earth. In the present study a plane-wave (uniform) source field is assumed. At the low frequencies of interest in GIC problems (periods of 30 minutes or less), it is the large-scale resistivity distribution that determines the E-field amplitudes, phases and their surface distribution.

Assuming an external plane wave source field of frequency f, the induced electric field at the surface is given by the magnetotelluric relationship:

$$E_y(f) = [-Z(f)] B_x(f) \qquad \qquad …(2)$$

Where $Z(f)$ is the complex surface impedance and the (X, Y) electric and magnetic fields are orthogonal. The surface impedance is a function of frequency and the resistivity structure of the subsurface. Equation (2) assumes a one-dimensional (1D) Earth resistivity structure; when the structure is more complex (e.g. 2D and 3D) the horizontal field components are coupled and related by a 2x2 impedance tensor.

In magnetotelluric calculations, the skin-depth determines the appropriate scale lengths for the problem. The skin-depth is defined as the depth across which the induced E-field is reduced in amplitude by $1/e$ from the surface amplitude. In resistive terranes (say 500 to >1000 ohm.m), the entire crustal and upper mantle environment (to a depth of several hundred km) will contribute to the surface response. The large scale lengths of the inducing fields involved in GIC effects also require that the offshore (seawater) domain be considered. Seawater is highly conductive when compared to all geological materials and provides far greater attenuation.

For a given resistivity distribution, the amplitude of the surface electric field will be frequency dependent. Taking a 100 ohm.m half-space as an example, the induced electric field would be about 3.5 mV/km.nT at a period of 1 minute. As the period increases to 10 minutes, the surface amplitude would reduce by a factor of about 3. As the period further increases to 30 minutes, the surface amplitude would reduce by a further factor of 2. Such frequency dependent effects indicate that the choice of inducing frequency is a critical factor in determining absolute magnitudes of the surface electric field. In terms of risk analysis, and for identical magnitudes of inducing fields, the highest frequencies produce the largest E-field amplitudes. In order to demonstrate the effect of frequency, modelling calculations have been performed at inducing periods of 10 and 30 minutes.

3.2 Development of a 3D resistivity model.
The geological classification of rocks bears only a tenuous relationship to their intrinsic resistivity. In addition, the vertical sensitivity of the E-field response for the GIC problem extends to depths in excess of 100 km. These two facts suggest that defining an appropriate 'national-scale' resistivity model is a non-trivial exercise. Some degree of simplification is inevitable. For the reworked crustal material of much of Britain, an appropriate method is to use a tectonic base map approach. The tectonic map of Britain (BGS, 1996) is available digitally at 1:1.5M and includes the offshore domain, the coastline and the whole of Ireland. The map defines nine orogenic terranes whose scale is likely to be more appropriate to the construction of a resistivity map to crustal scale (and greater) in the first instance.

In order to allow for electromagnetic boundary effects (see later), the resistivity model was specified over an area of 1100 by 1200 km. Six major terranes were identified from the tectonic map. The terranes, from north to south, included the Northern Highlands, the Central Highlands, the Midland Valley, the Southern Uplands, the Concealed Caledonides and the Variscide terrane (see later Figure 9b). The model was developed on the basis that lateral resistivity effects, both onshore and offshore were confined to the boundaries between the six zones. The only other lateral resistivity boundary specified within the model was that due to seawater i.e. the coastline.

It is important to note that skin-depths for the GIC problem indicate that it is the bulk conductivities, averaged vertically over tens of kilometres, to depths of several hundred kilometres that primarily influence the magnitude of the E-field at the surface. Localised perturbations may arise due to near-surface lateral resistivity contrasts but the vertical distribution requires only a gross specification.

In the study undertaken, three vertical zones (0-10, 10-20, 20-30 km) were used to allow for crustal scale resistivity variations in each of the six terranes. Below the crustal scale it is more appropriate (due to lack of information) to adopt a regionally representative 1D model. The most obvious sources of deep resistivity information are the results of magnetotelluric (MT) surveys. Various MT studies, conducted with increasing sophistication largely through the 1970s and 1980s, have covered mainland Scotland and northern England (Hutton et al., 1981; Livelybrooks et al., 1993). The studies have identified a variety of crustal scale resistivity zones which, importantly, have contrasts at the boundaries of the terranes (e.g. the Great Glen Fault, the Highland Boundary Fault and the Iapetus Suture zone). To the south of the Alston Block of northern England there is almost a total absence of deep resistivity information. Of particular note is the absence of deep information on the concealed Caledonide basement. Data from two BGS surveys south of the Variscan front were used. The simplified resistivity zonation used should be considered representative rather than an actual distribution of resistivity.

A 1D resistivity model extending from 30 to 1000 km underlies all six zones. The model is developed from long period observations from observatory data (Schultz and Larsen, 1990). Both layered and smoothly-varying models may be defined; our preferred model is a smooth distribution in which resistivity decreases monotonically to a minimum value at the maximum depth (e.g. Olsen, 1998).

3.3 Numerical modelling.

Recent advances in 3D plane-wave modelling using finite-difference equations are described by Mackie et al. (1993). A description of the algorithm used here is provided by Mackie et al. (1994). The algorithm computes the surface fields of general 3D models using the minimum residual relaxation method. Model construction uses a 3D 'core' (in x, y and z) with 2D extensions (in x,z and y,z) at the edges of the core. (Note that here x represents an east coordinate, y represents a north coordinate, which is opposite to the normal convention for defining magnetic field components, used in the previous section, where X is the north component and Y is the east component.) The 3D core and 2D extensions are underlain by a 1D 'base'. All three model elements are constructed using a staggered grid that must conform to skin-depth requirements.

No single set of cell constructions can accommodate both skin-depth requirements and the scale of onshore/offshore Britain without becoming computationally unwieldy. A 20x20 km lateral grid model of the British Isles was developed for the initial evaluations described here. The results were obtained using a 55 by 60 cell (each 20x20 km) core model that runs from –300 to 800 km (Ordnance Survey British National Grid Easting) and from –100 to 1100 km (Northing). The coastline and tectonic zones of the digital model are shown in Figures 9a and 9b. The model is crude and obviously capable of

refinement. Skin depth algorithm requirements mean that a realistic sea-water resistivity of 0.25 ohm.m cannot be used for a 20 km lateral grid at the higher frequencies considered (600 s). A sea-water resistivity of 4 ohm.m has been used. This has only a marginal effect in a 1D sense but it produces lower amplitude lateral effects at the coastal boundary (the resistivity contrast is lower by a factor of 16). The model results presented here are for variation fields with periods of 30 and 10 minutes. The results presented use a unitary inducing H-field boundary condition of 1 A/m at the surface; this corresponds to a *B*-field amplitude of 1257 nT. The unitary boundary condition is specified along the leftmost surface edge of the model where no perturbations due to lateral contrasts in resistivity structure occur.

The 2D and 3D model components extend to a depth of 30 km (i.e. the crustal scale) using 8 layers. The 8 layers increase in thickness from an initial layer thickness of 200 m. The initial layer was used to incorporate the average thickness of the shelf seas. The modelling is plane-wave and therefore field polarisation must be defined. The standard terminology of *Ex* polarisation indicates that a N-S magnetic oscillation (*Hy*) drives an E-W electric field. The orthogonal *Ey* polarisation indicates that an E-W magnetic oscillation (*Hx*) drives a N-S electric field. In a 3D model, a polarised inducing field provides both *Ex* and *Ey* components at resistivity boundaries; the modulus of the vector resultant is used for display.

3.4 Results of numerical modelling

A number of results for different resistivity distributions were obtained as preliminary investigations. The preliminary models included models with no coast (ie. a uniform 200m upper layer) and with coast only (ie. no geological terranes). Such baseline models allow a comparison of the magnitudes of the different lateral effects across the landmass. Electric fields for any given linear azimuth can be obtained. The results for the *Ex* polarisation (an E-W regional electric field produced by an oscillating N-S magnetic field) probably have the most relevance to the GIC problem across the British Isles. This is because the external electric field during storm time conditions has a strong E-W component. In plane-wave modelling, results for other external field azimuths may be obtained by combining (vector addition) the fields from two orthogonal, linear polarisations.

Figure 10a shows the surface electric fields obtained using the specified 3D model. The results shown are for the *Ex*-polarisation at a period of 30 minutes. The background (i.e. no lateral perturbations) amplitude level is 653 mV/km (offshore) and 670 mV/km (onshore). The maximum and minimum values in Figure 10a are 2212 and 14 mV/km respectively. The main perturbations to the induced E-field are clearly caused by the coast effect. E-field magnitudes are reduced offshore and enhanced onshore with respect to background (1D) levels. The shallow (coastal boundary) effects are large and localised while crustal scale resistivity contrasts produce smaller amplitude but larger scale effects. The largest effects produced by the tectonic terrane model occur where the model has the highest resistivity contrast (the NW of Scotland).

The results for the same model and polarisation at an inducing period of 10 minutes display a similar distribution to those of Figure 10a. Due to the higher frequency however, the background amplitude level increases to 1309 mV/km (offshore) and 1345 mV/km (onshore). Localised high amplitude effects again occur onshore and exceed 4000 mV/km. Field polarisation can play a significant role in the distribution of induced fields. Figure 10b shows the results for the *Ey* polarisation at a period of 10 minutes. Maximum and minimum values are 4395 and 87 mV/km respectively.

The precise effects of the high value assigned to the sea water resistivity would be best estimated in future 3D modelling by decreasing the cell sizes and increasing the number of cells. Typical computation times for such models would remain modest (less than 1 hour). Although the main focus here has been the estimation of surface *E*-fields for the engineering calculation (equation 1), the modelling results can be compared with field observations to test their validity. The behaviour of low frequency induction vectors (vertical to horizontal magnetic field ratios) offer a means of summarising the *integrated* effects of the induced currents from *both* polarisations of the inducing field. Induction vectors are defined by their amplitude, phase and azimuth. Real induction vector magnitudes (G_R in the notation of Beamish, 1985) calculated for a period of 10 minutes are shown in Figure 11. The diagram shows the contoured magnitudes, expressed as a percentage, together with the real induction arrows that point towards excess concentrations of current caused by lateral resistivity contrasts. Amplitude is also incorporated into the size of the arrows; the maximum arrow size is 4.5%. In the south and south-east, where no crustal scale resistivity contrasts are defined in the model, a simple coast-effect behaviour is observed. The high contrast tectonic terrane boundaries in Scotland produce the largest induction vectors and provide some complex rotation patterns. Equivalent observations of induction vectors across the British Isles, although sparse, are presented by Beamish (1985) for a frequency range then encompasses that of the present modelling study. The observations indicate that real induction vector magnitudes should reach (typically) minimum values of between 10% and 20%. The largest observed magnitude in Figure 11 is only 4.5%. The comparison suggests that the model parameters used, do not generate sufficient excess concentrations of current in both geological and coastline contexts.

4. Conclusions

From the results presented here we can draw some general conclusions:

1. Magnetic storms exceeding an HSD threshold of 50 nT at all three UK magnetic observatories may occur up to 10 times a year in years of maximum magnetic activity, and may still occur during years of low magnetic activity.

2. Geomagnetic disturbances that may give rise to GICs in the UK power grid tend to occur in the night-time hours. There is also a tendency for a greater occurrence of high activity in March and October. This is consistent with the behaviour of more 'traditional' geomagnetic indices such as *Ap* and *aa*. Most periods of significant magnetic activity last less than 3 hours.

3. The study has discussed the behaviour of the horizontal *E*-field induced across the British Isles by external geomagnetic variation fields. It has been pointed out that, for the same inducing field magnitude, the highest frequencies produce the largest surface *E*-fields and therefore provide the highest risk in terms of induced GIC amplitudes. At the frequencies appropriate to the GIC problem, it is the deep (> 30 km) upper mantle resistivity distribution that largely determines the amplitude level of the surface fields. Both of these statements are strictly applicable to a resistivity distribution that varies only with depth. Such a distribution is unrealistic.

4. When lateral resistivity gradients are considered, currents are generated which provide a redistribution of the amplitude and phase of the surface electric fields. The results of the modelling presented here demonstrate the spatial complexity that may be expected in the GIC problem across the British Isles. Onshore enhancement by factors of between 2 and 4 in the induced electric field are a pervasive feature. The fields are not spatially uniform particularly for grid elements at coastal locations. In order to implement preliminary but accurate 3D modelling, the resistivity of seawater has been taken to be a factor of 16 above the realistic value (0.25 ohm.m). The precise effects of the high value assigned to the sea water resistivity would be best estimated in future 3D modelling by decreasing the cell sizes and increasing the number of cells.

In order to improve both the modelling and monitoring aspects two further developments can be considered (both of which may make direct use of data from the UK magnetic observatories):

1. There needs to be a more systematic, long-term monitoring of GICs in the neutral line of UK power transformers, especially at coastal sites. Comparison with theoretical models of GICs may lead to improvements in electric field and network current models and may improve the likelihood of accurate real-time monitoring and forecasting.

2. Improved electrojet models, e.g. the models of Boteler and Pirjola (1998) and Pirjola and Viljanen (1998), are important for a more physically realistic surface electric field model leading to, again, accurate modelling of network currents and potentials.

Finally, we note that the coastal effect may have implications beyond the power industry, for example, for pipeline operations at coastal sites around the world at near-auroral latitudes.

Acknowledgements

References

Beamish, D., 1985. The frequency characteristics of anomalous vertical fields observed in the British Isles. *J. Geophys.*, 57, 207-216.

BGS, 1996. Tectonic map of Britain, Ireland and adjacent areas. Pharaoh, T.C., Morris, J.H., Long, C.B. (compilers). 1: 1 500 000 (Keyworth, Nottingham: British Geological Survey).

Blais G. and Metsa P., 1994. Operating the Hydro-Quebec grid under magnetic storm conditions since the storm of 13 March 1989. *In Solar-Terrestrial Predictions IV, Proceedings of a Workshop at Ottawa, Canada, Department of Commerce, USA, 108-130.*

Boteler D. H., 1998. The relation between magnetic range and spectral power. *Geophys. J. Int.,* 134, 613-616.

Boteler D. H. and Pirjola R. J., 1998. The complex-image method for calculating the magnetic and electric fields produced at the Earth's surface by the auroral electrojet. *Geophys. J. Int.*, 132, 31-40.

Cagniard L., 1953. Basic theory of the magneto-telluric method of geophysical prospecting. *Geophysics*, 18, 605-635.

Hutton, V.R.S., Dawes, G., Ingham, M., Kirkwood, S., Mbipom, E.W. and Sik, J., 1981. Recent studies of time variations of natural electromagnetic fields in Scotland. *Phys. Earth Planet. Int.,* 24, 66-87.

Joselyn, J.A., Anderson J.B., Coffey H., Harvey K., Hathaway D., Heckman G., Hildner E., Mende W., Schatten K., Thompson R., Thomson A. W. P. and White O. R., 1997. Panel achieves consensus prediction of Solar Cycle 23. *EOS, Trans. Amer. Geophys. Union*, 78, pages 205, 211-212.

Livelybrooks, D., Banks, R.J., Parr, R.S. and Hutton, V.R.S., 1993. Inversion of electromagnetic induction data for the Iapetus Suture Zone in the UK. *Phys. Earth Planet. Int.*, 81, 67-84.

Mackie, R.L., Madden, T.R. and Wannamaker, P.E., 1993. Three-dimensional magnetotelluric modeling using difference equations - theory and comparisons to integral equation solutions. *Geophysics*, 58, 215-226.

Mackie, R.L., Smith, J.T. and Madden, T.R., 1994. Three-dimensional electromagnetic modeling using finite difference equations: the magnetotelluric example. *Rad. Sci.*, 29, 923-935.

Olsen, N. 1998. The electrical conductivity of the mantle beneath Europe derived from C-responses from 3 to 720 hr. *Geophys. J. Int.,* 133, 298-308.

Pirjola R. and Viljanen A., 1998. Complex image method for calculating electric and magnetic fields produced by an auroral electrojet of finite length. *Ann. Geophys.* **16**, 1434-1444.

Schultz A. and Larsen J., 1990. The electrical conductivity of the mid-mantle:II. Delineation of inhomogeneity by application of extremal inverse solutions. *Geophys. J. Int.,* 101, 565-580.

Smith P. M., 1990. Effects of geomagnetic disturbances on the national grid system. *Universities Power Engineers Conference, Aberdeen.*

Viljanen A., 1997. The relation between geomagnetic variations and their time derivatives and implications for estimation of induction risks. *Geophys. Res. Let.,* 24, 631-634.

Viljanen A. and Pirjola R., 1994. Geomagnetically induced currents in the finnish high voltage power system. *Surveys in Geophysics,* 15, 383-408.

Figure Captions

Figure 1. The locations of the three magnetic observatories in the UK, and the substation at Neilston where GICs (see Figure 2a) were recorded on 17-18 November 1989.

Figure 2. (a) Pen-chart recording (courtesy of R. Paton, Scottish Power plc, 1992) of GICs measured in the earth-line of a Neilston transformer on 17th November 1989. An approximate UT time-scale is shown on the bottom of the plot. The three traces represent three measurements of the same GIC with different instruments. Each major vertical division (or 'box') represents 5A and each horizontal division represents one hour. The three traces are not time-synchronous, as can be seen by the offsets in the timing of the sudden commencement at the left-hand edge of the plot. (b) Rate of change, in nT/minute, of the North (X) component of the geomagnetic field at the three UK observatories (Lerwick, Eskdalemuir and Hartland) for the storm of 17-18 November 1989. Scales denoted by figures on the left- and right-hand sides.

Figure 3. (a) The hourly standard deviation in the North (X) component of the field at the UK observatories for the storm of 17-18 November 1989. (b) As (a), but for the East (Y) component of the field.

Figure 4. The maximum hourly standard deviation per day at the three UK observatories for the period 1983-1999 in the X and Y components of the field. Lerwick is shown in red, Eskdalemuir in green and Hartland in blue.

Figure 5. The annual distribution of magnetic storms in the *X* (North) component of the field, and defined by the 50 nT threshold described in the text, for the three UK observatories. The *Y* component shows a similar distribution but has typically fewer occurrences compared with *X*.

Figure 6. The distribution of 'GIC-type' storm duration times in the *X* (North) component of the field in the UK. The *Y* component shows a similar distribution but has typically fewer occurrences compared with *X*.

Figure 7. The distribution in universal time of the occurrence of 'GIC-type' storms, in the *X* (North) component of the field in the UK. The *Y* component shows a similar distribution but has typically fewer occurrences compared with *X*.

Figure 8. The seasonal distribution of the occurrence of 'GIC-type' storms in the *X* (North) component of the field in the UK. The *Y* component shows a similar distribution but has typically fewer occurrences compared with *X*.

Figure 9. Lateral boundaries of the 3D model core comprising 55 (BNG –300 to 800 km) x 60 (BNG –100 to 1100 km) 20x20 km cells. (a) Coastline of the British Isles. (b) Six simplified tectonic terranes: NH=Northern Highlands, CH=Central Highlands, MV=Midland Valley, SU=Southern Uplands, CC=Concealed Caledonides and V=Variscides.

Figure 10. Results of 3D modelling. Electric field variations shown as a surface. Inducing magnetic field of 1 A/m. Vertical scale bar shows *E*-field amplitude in mV/km. (a) *Ex* polarisation at a period of 30 minutes. (b) *Ey* polarisation at a period of 10 minutes.

Figure 11. Induction vector magnitudes (G_R) and induction arrows calculated at a period of 10 minutes. Magnitudes, expressed in %, are contoured and arrows which point towards current concentrations are shown.
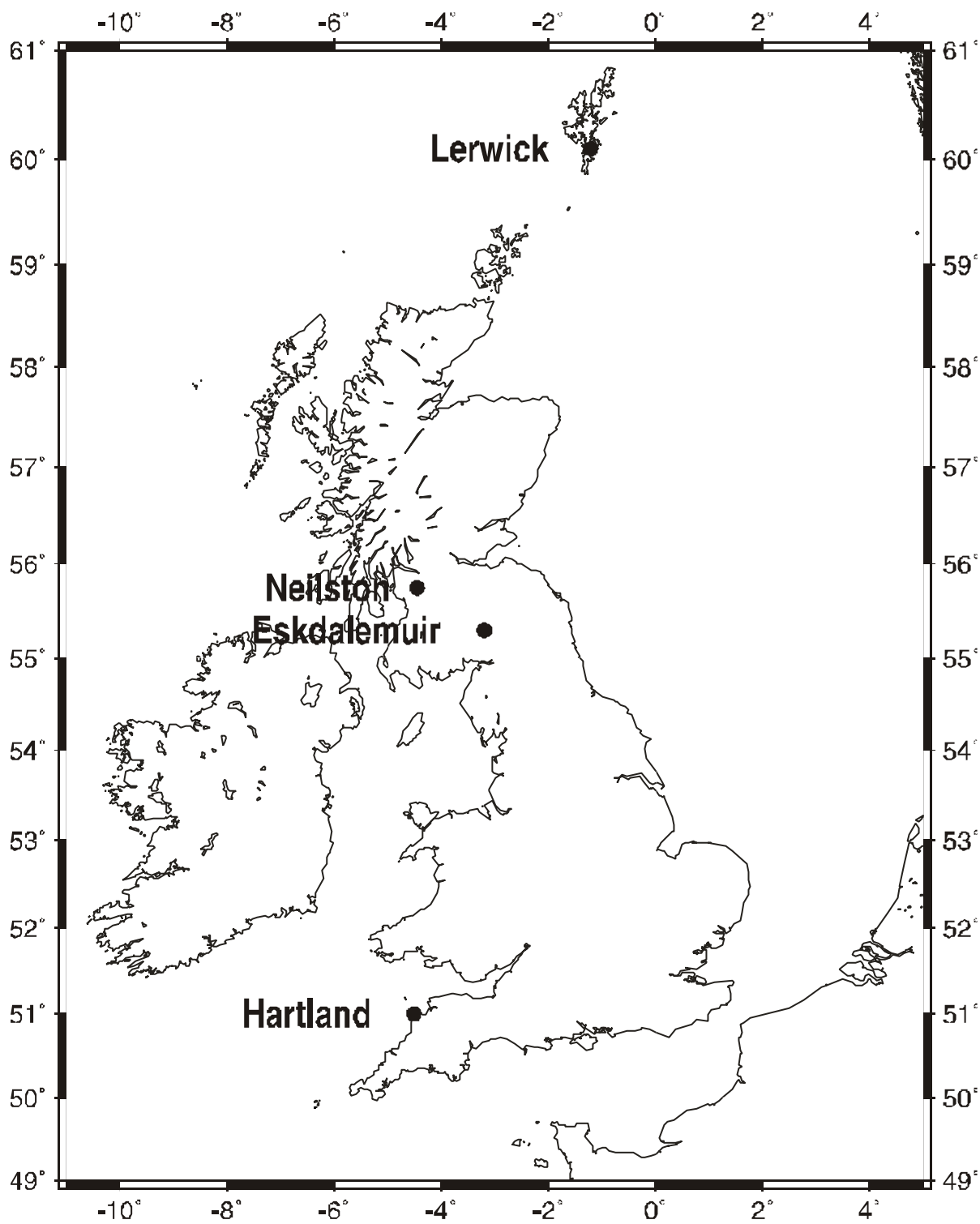
Figure 1
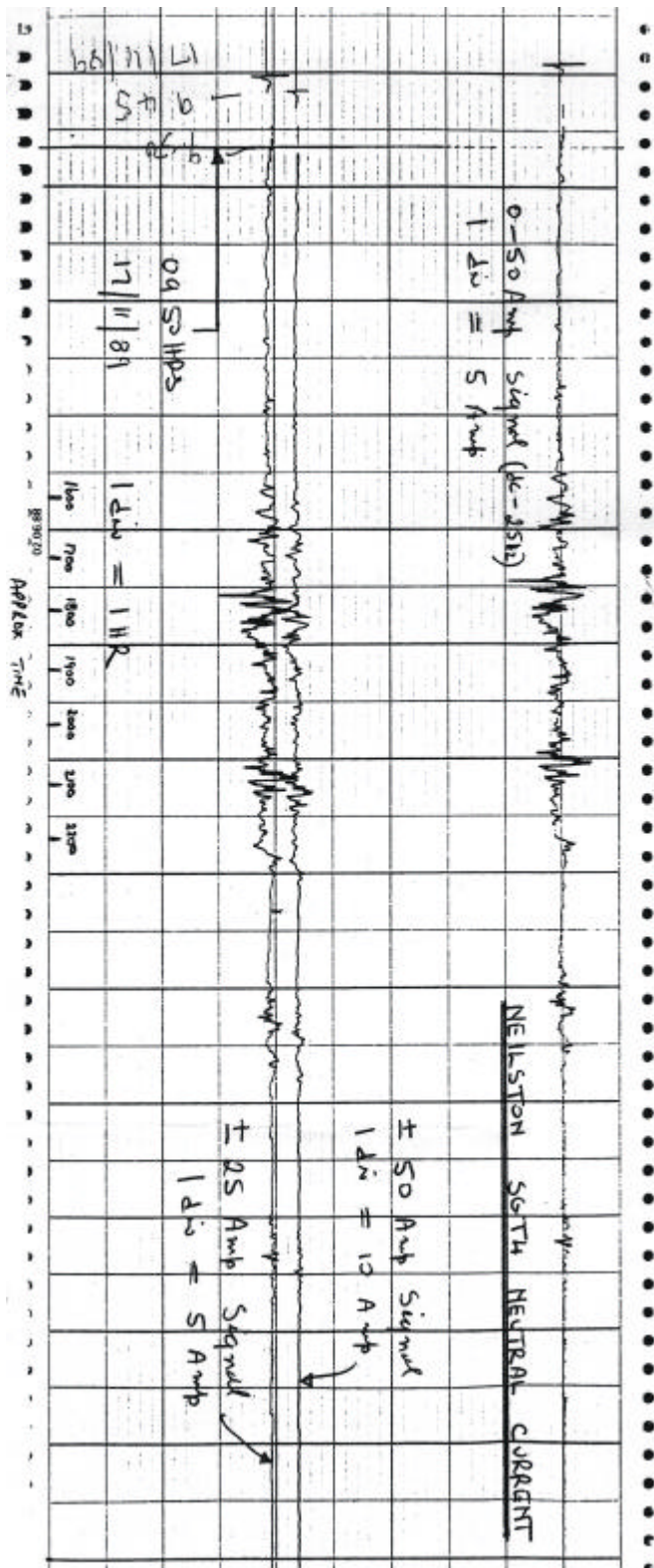
Figure 2a
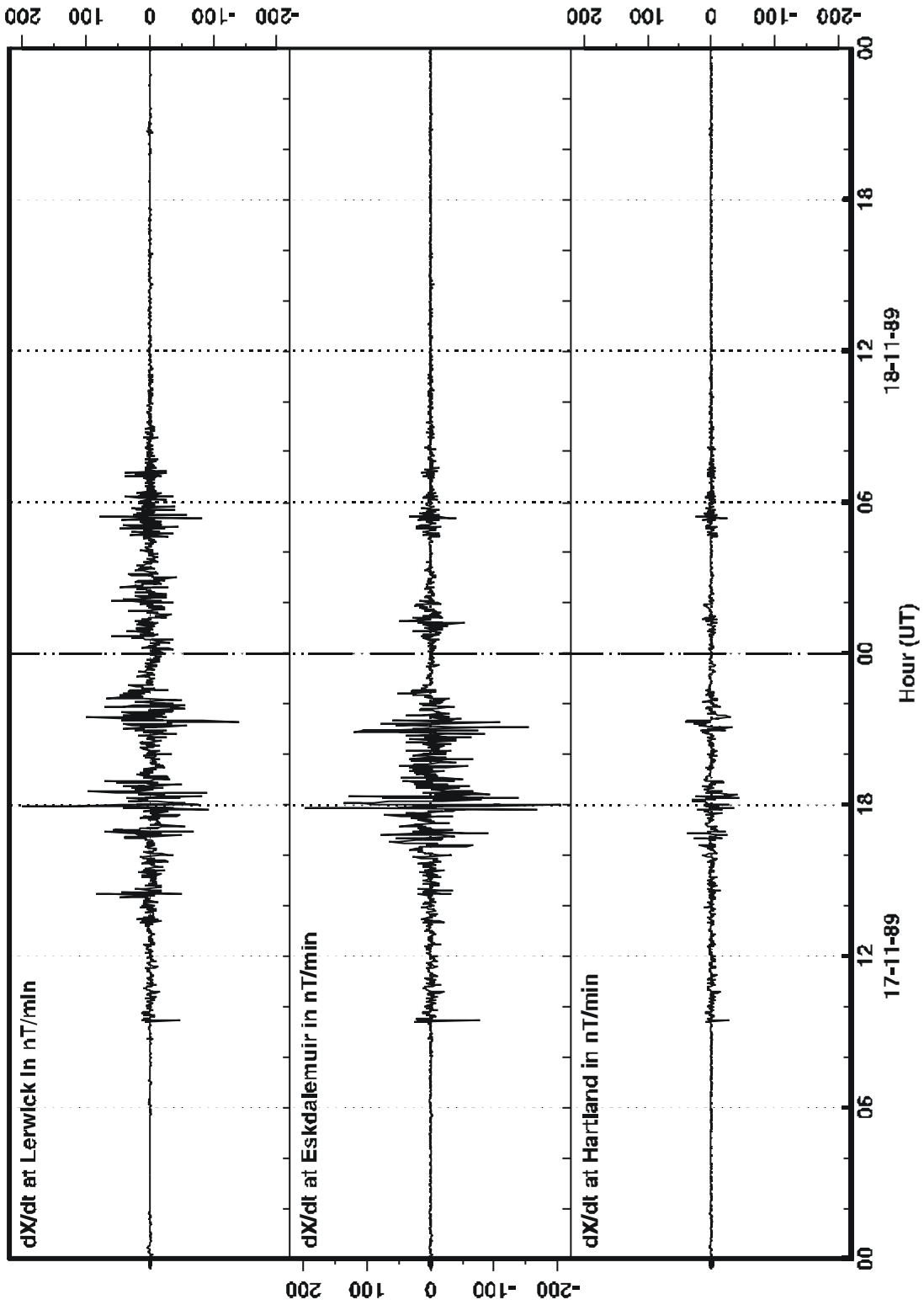
Figure 2b
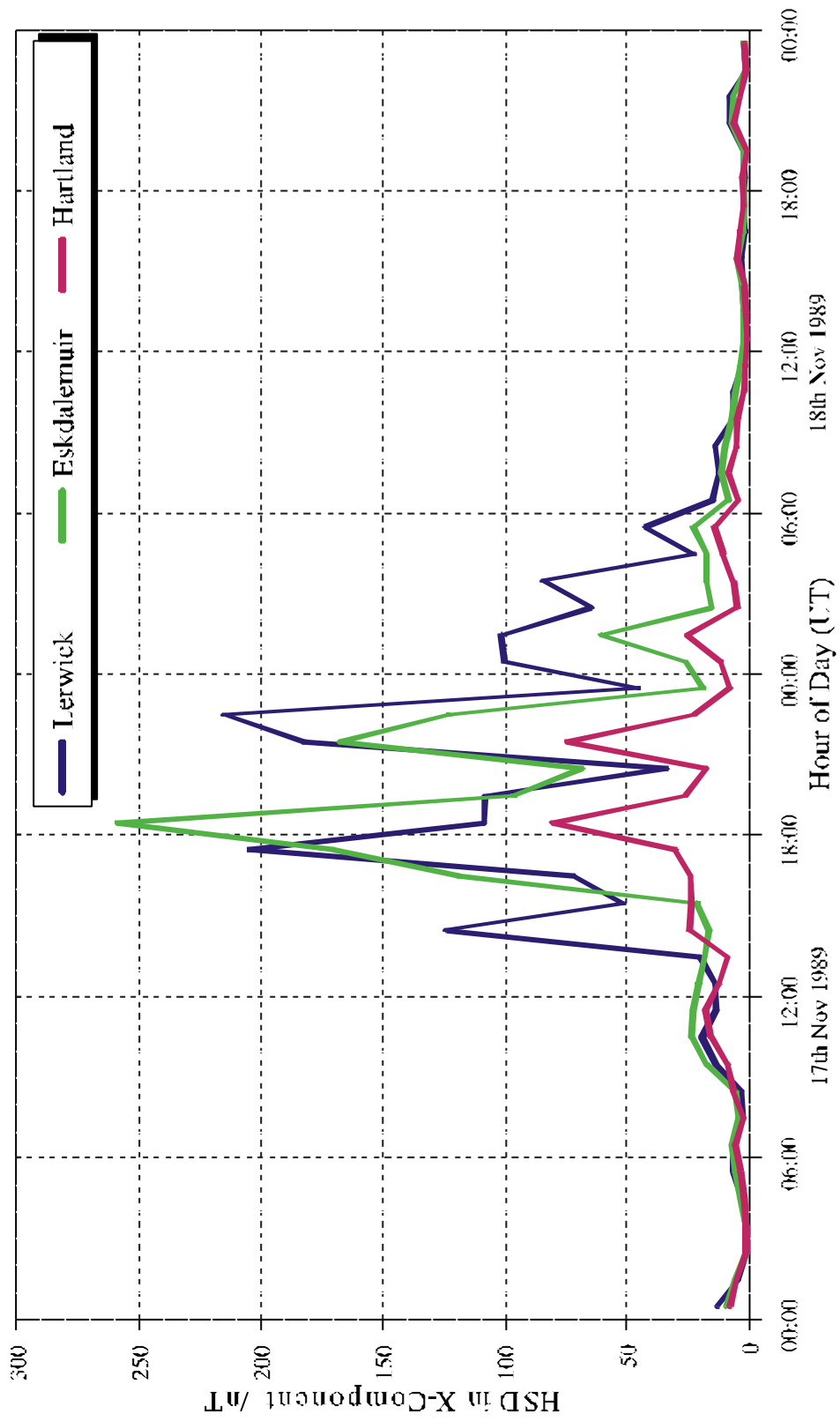
Figure 3a
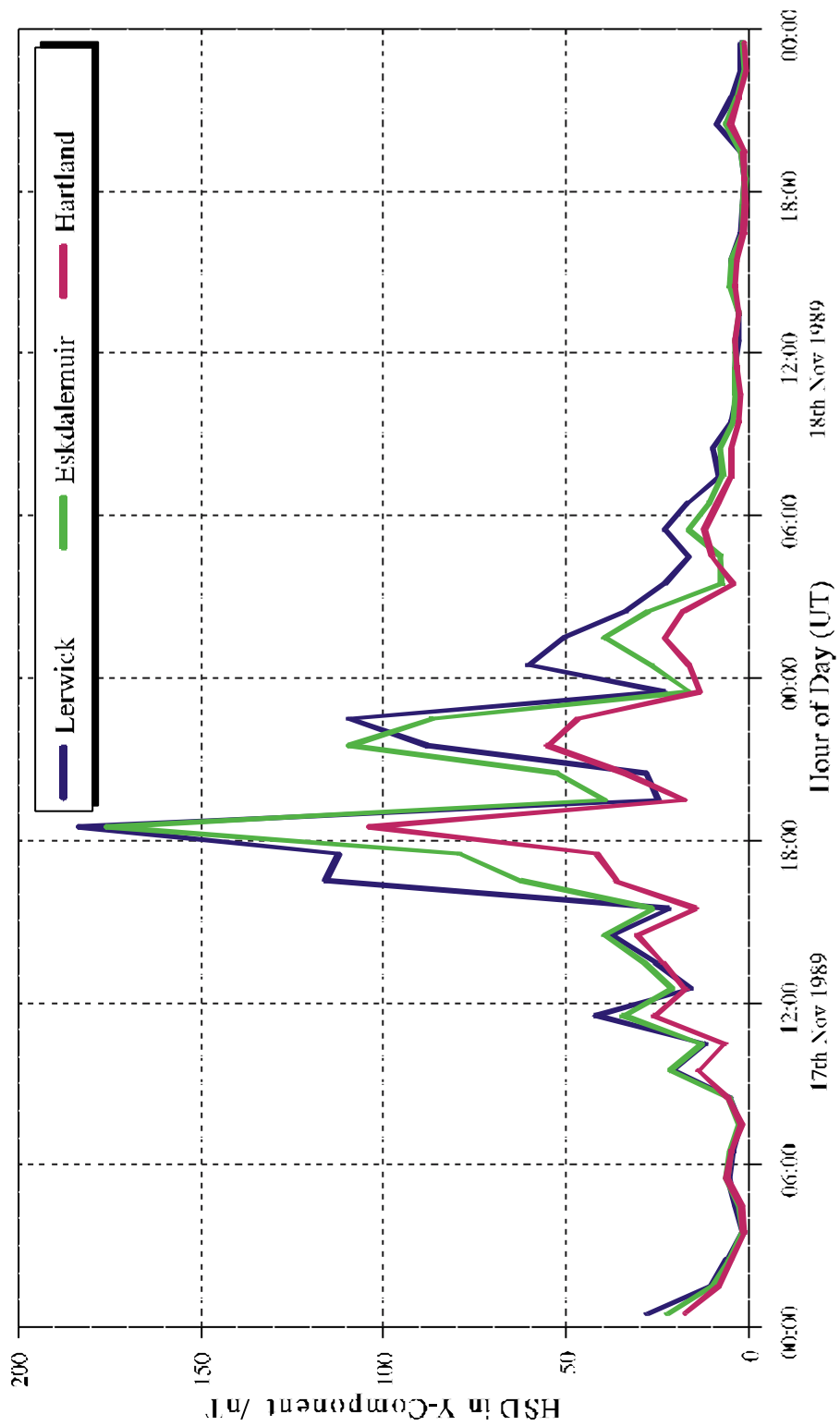
Figure 3b
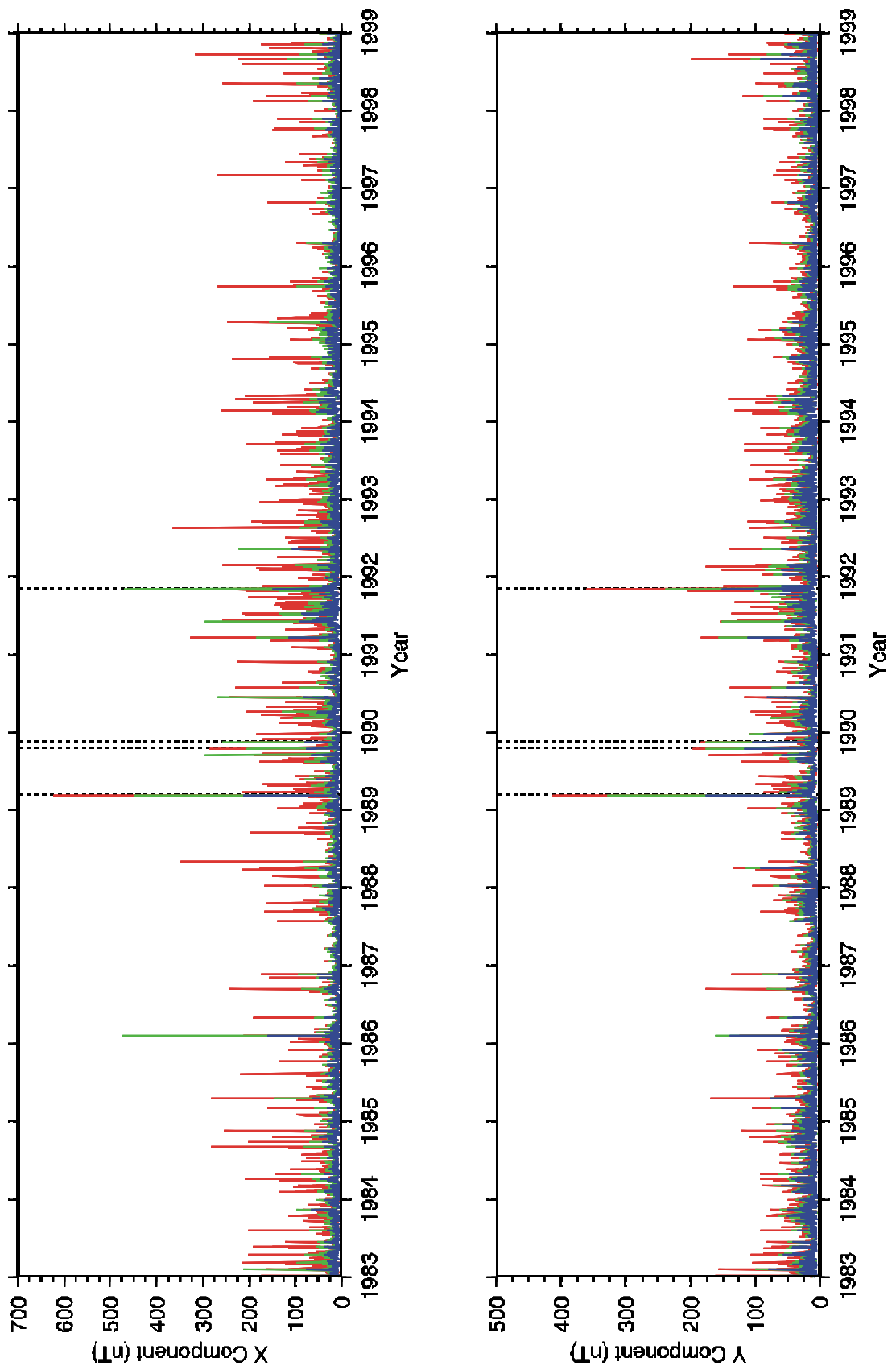
Figure 4
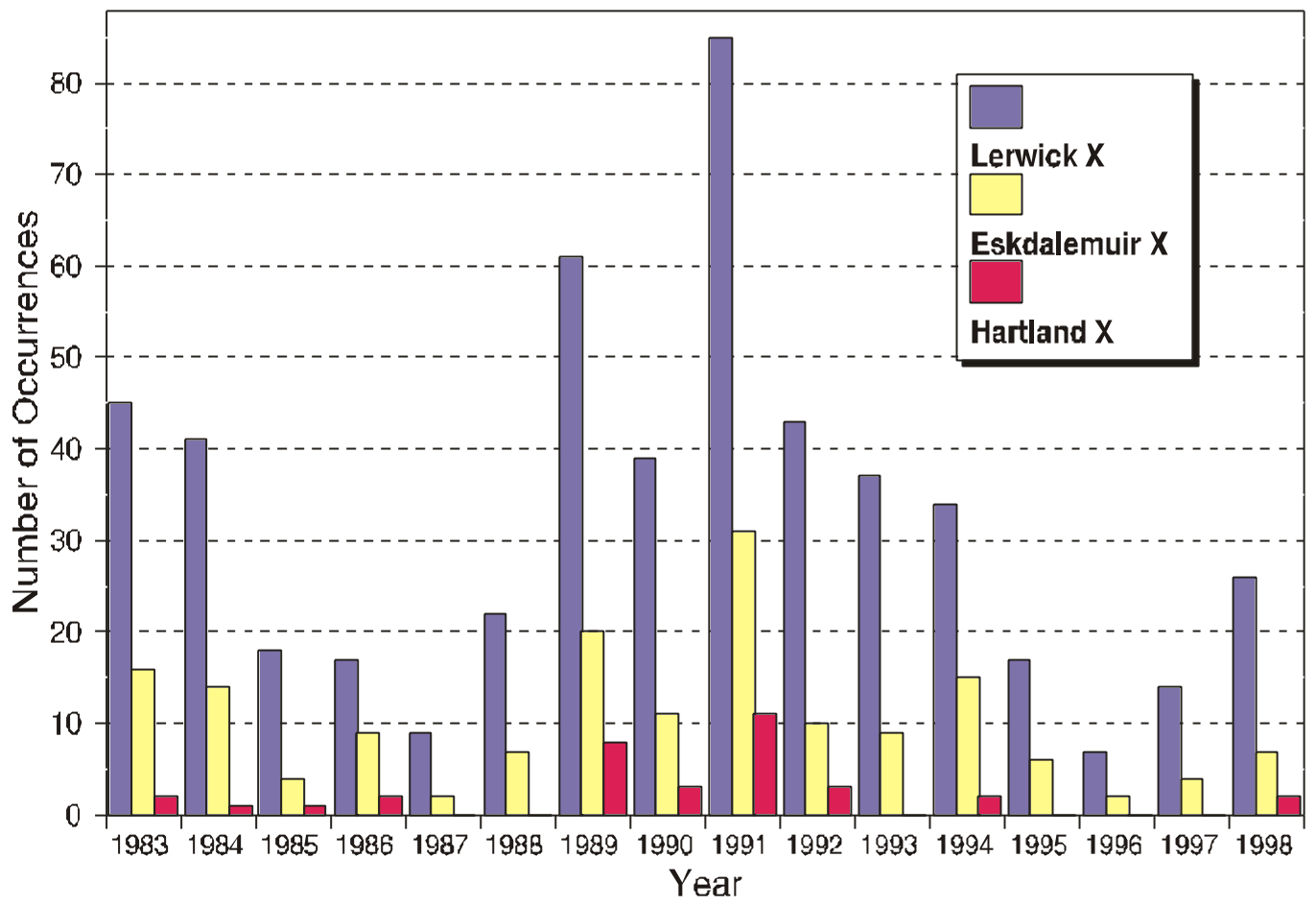
Figure 5
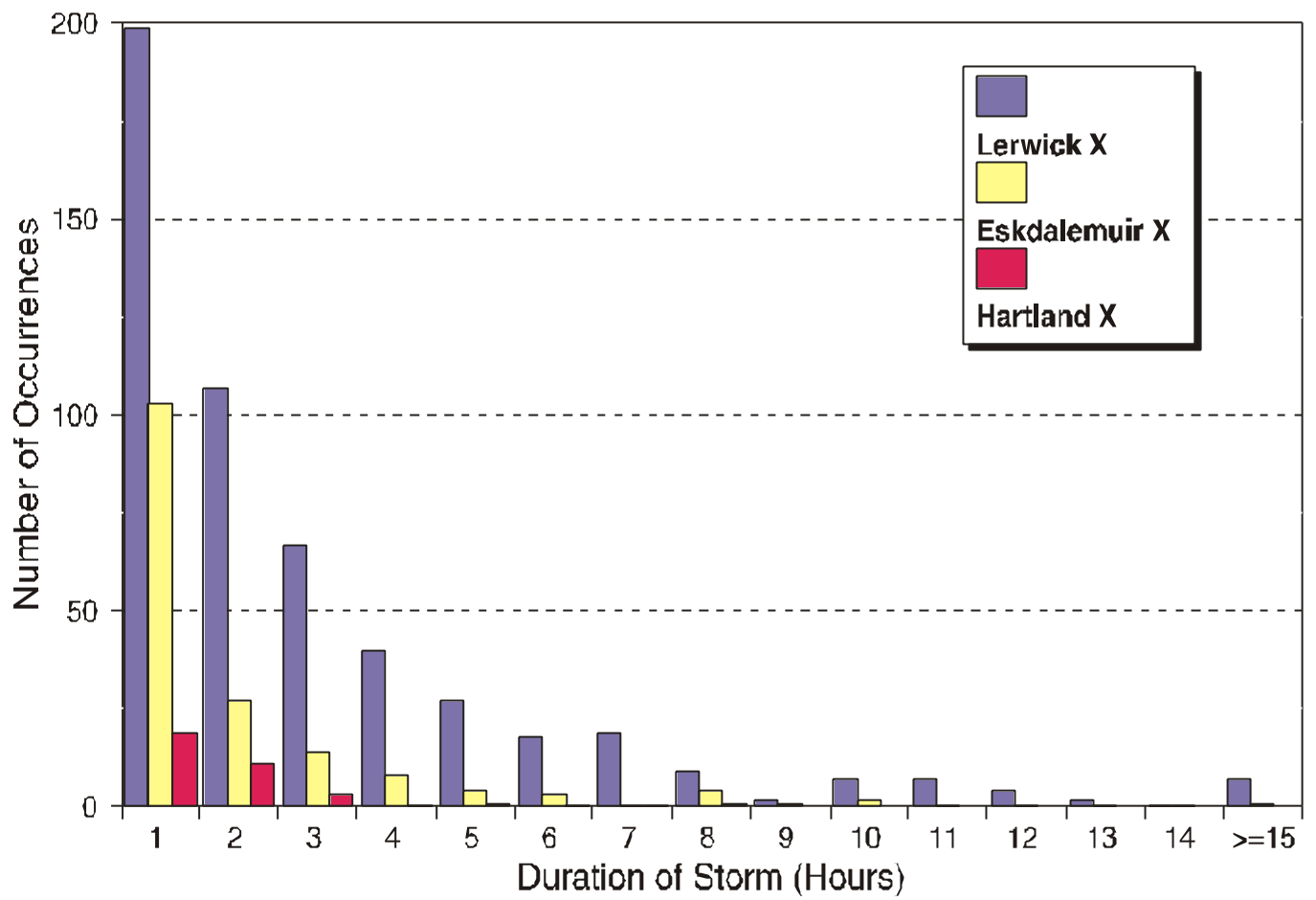
Figure 6
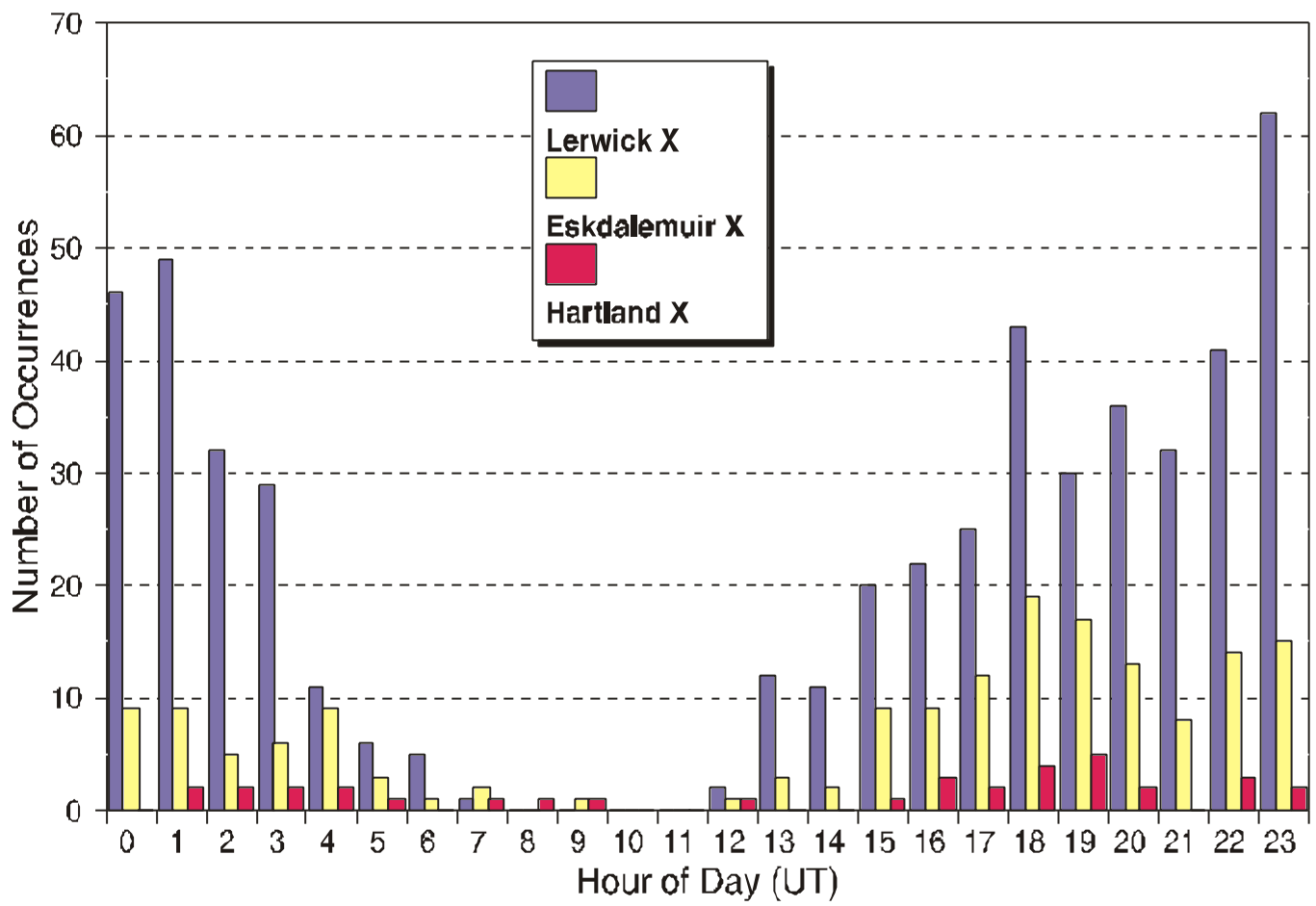
Figure 7
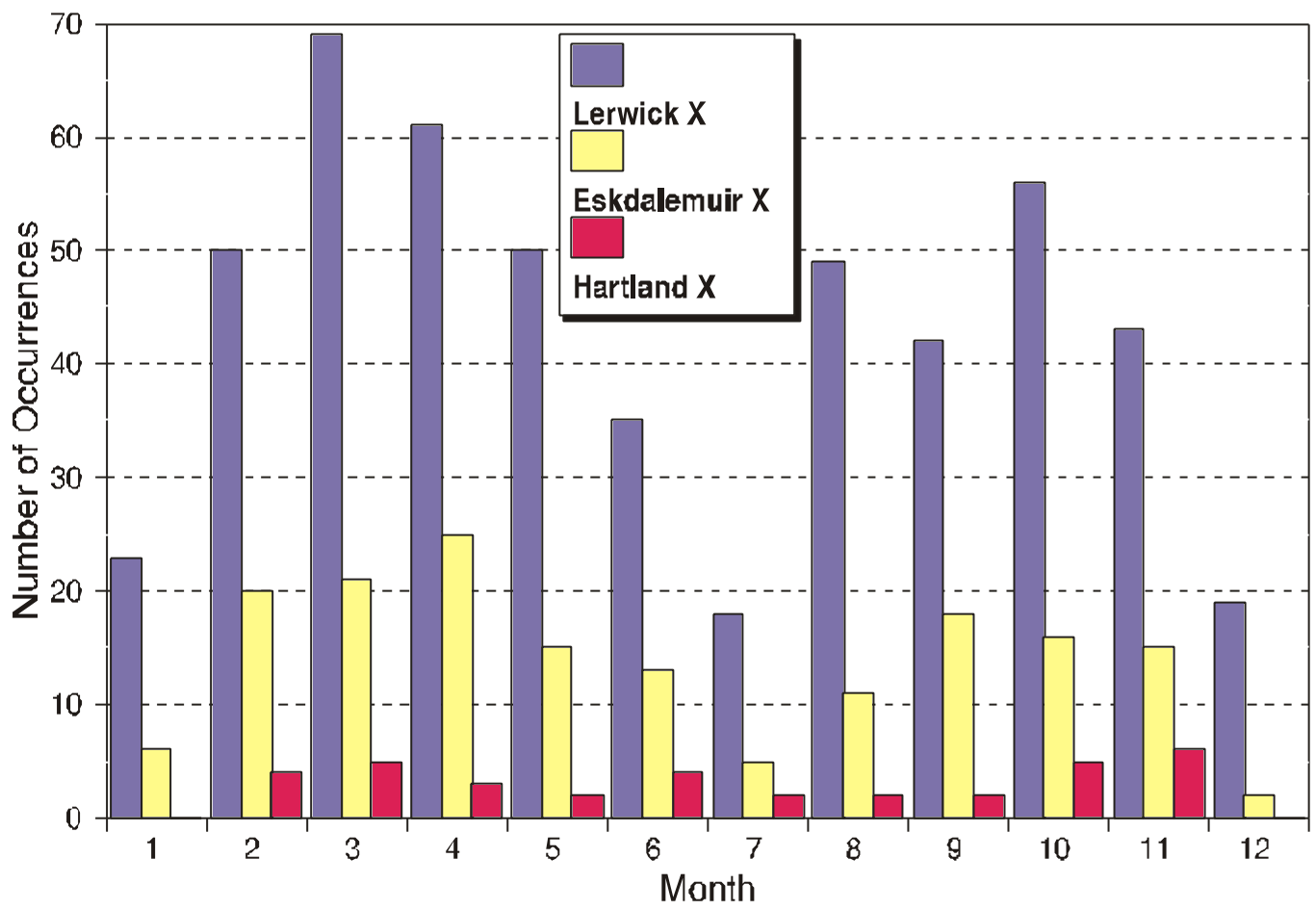
Figure 8
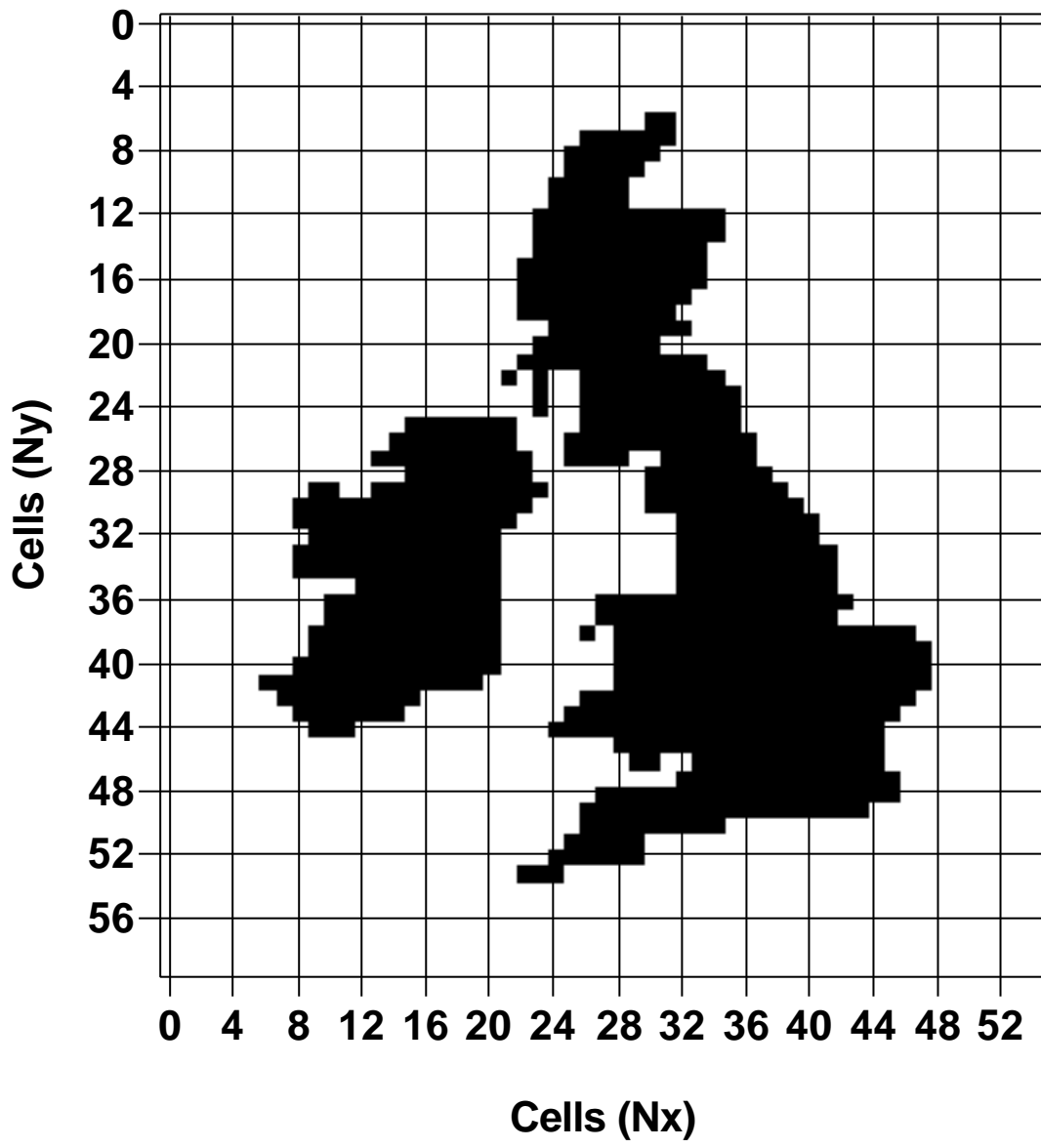
Figure 9a

Figure 9b

Ex-polarisation : 30 minute period

E-field (mV/km)

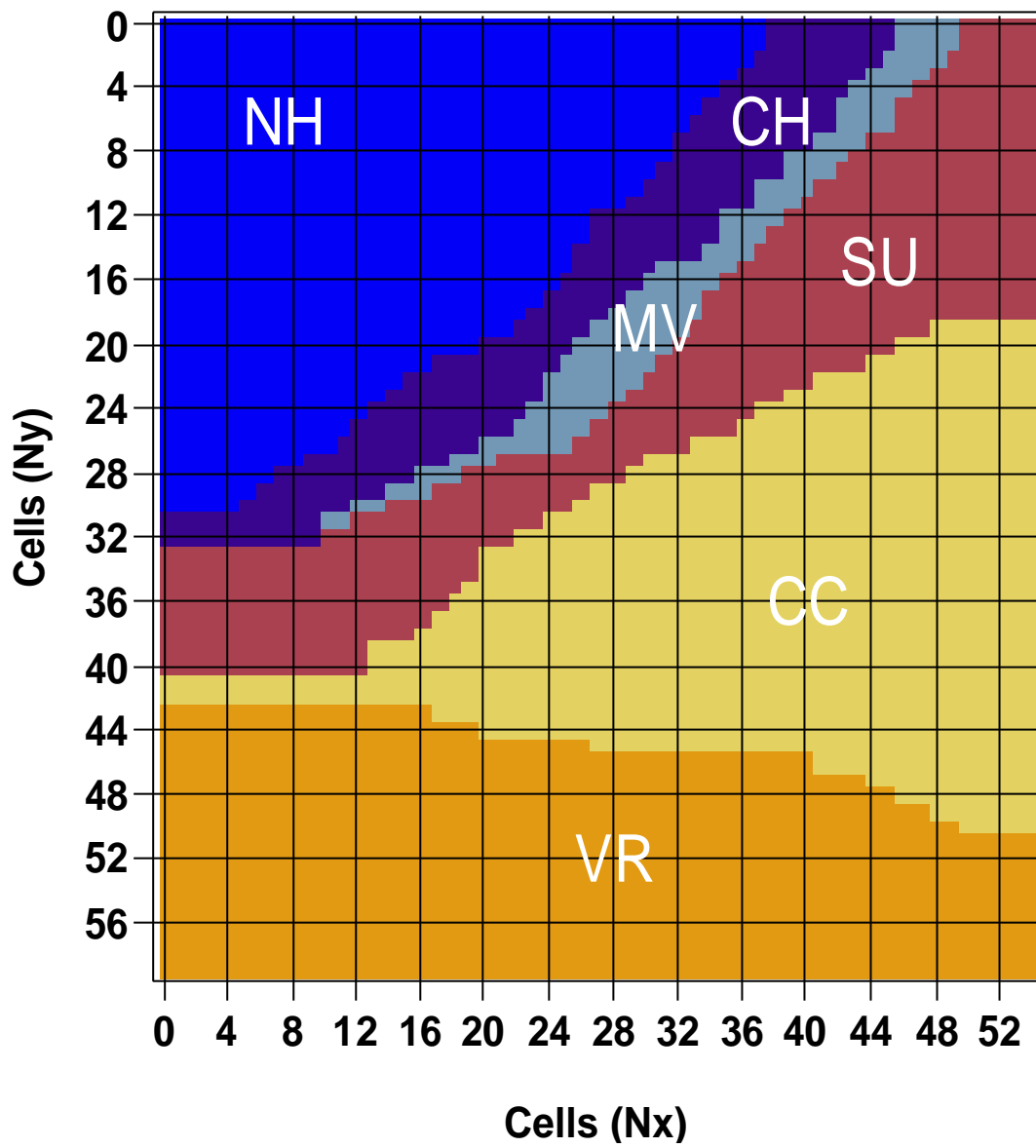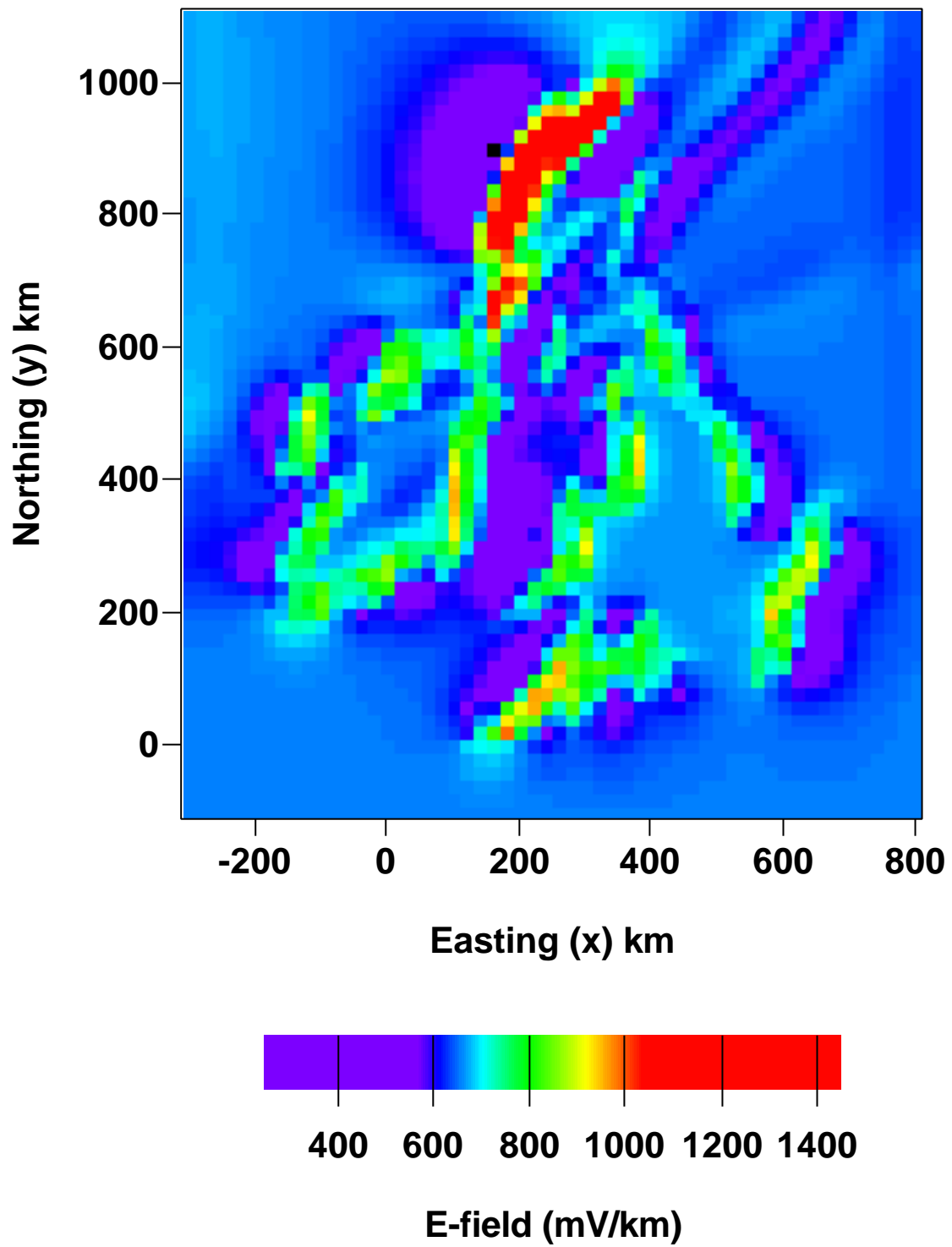**Figure 10a**

Ey-polarisation : 10 minute period

Figure 10b

Figure 11